Corrosion resistance of silicon-modified nitinol in artificial physiological solutions

A.I. Lotkov[1]*, S.G. Psakhie[1, 2], L.L. Meisner[1, 3], A.V. Korshunov[4], S.N. Meisner[1, 3], and V.M. Diamant[5]

[1] Institute of Strength Physics and Materials Science, Siberian Branch, Russian Academy of Sciences, Tomsk, 634021 Russia
[2] Skolkovo Institute of Science and Technology, Skolkovo, 143025 Russia
[3] National Research Tomsk State University, Tomsk, 634050 Russia
[4] National Research Tomsk Polytechnic University, Tomsk, 634050 Russia
[5] Lithotech Medical Ltd., Katzrin, 12900 Israel

Electrochemical methods were used to investigate the corrosion resistance of nitinol specimens modified with silicon by ion implantation (fluence $2 \cdot 10^{17}$ ions/cm^2). After ion beam treatment, nickel concentration in the surface layer is significantly reduced up to ~20 nm deep and a silicon-containing layer is formed at the depth of 10...80 nm with the maximum concentration of 30 at % at the depth of 30...35 nm. The breakdown (pitting) potential E_b of such NiTi–Si specimens in 0.9% NaCl physiological solution and in artificial blood plasma is ~0.9 V (Ag/AgCl/ KCl sat.) which is much higher than E_b of test specimens subjected to mechanical, chemical or electrochemical treatment. It is shown that under potentiostatic conditions at E_b the NiTi–Si specimen surface is stable to failure and does not exhibit pitting, spotting or microcracking. The comparison of corrosion test results with the cyclic voltammetry data for NiTi, Ti and Ni as well as with thermodynamic calculations demonstrates that the surface of the modified NiTi–Si specimens has enhanced stability with respect to the release of nickel ions into solutions.

Keywords: nitinol, ion implantation, silicon-modified surface, artificial physiological solutions, corrosion

1. Introduction

Among the shape memory materials based on copper, iron, nickel or titanium [1], only the near equiatomic NiTi alloys have been used, mainly under the trade name nitinol (NiTi), in biomedical applications such as endoluminal stents in cardiology, urology and gastroenterology, as orthodontic wires in dentistry, as tissue connectors, as spring rods for scoliosis correction and many more [2–4]. NiTi alloys possess high yield, tensile, and fatigue strengths and high elastic-plastic characteristics, exhibit shape memory and superelasticity and are capable of substantial strain accumulation (ε = 4–6 %) and reversible strain recovery without failure [5–7].

The high amount of the allergenic and toxic element Ni [8–14] in the NiTi alloys and its potential release into the body [15–18] are at the centre of attention when considering the surface treatment as part of general manufacturing. To improve the biocompatibility of implant devices, predominantly those in contact with blood, it suffices to provide these properties on the surface or in thin surface layers. Efficient methods of improving the physical-chemical and mechanical properties of implant surfaces and their biocompatibility are based on ion beam and ion plasma surface treatment [19–22]. Such surface modification of NiTi devices may change the mechanical characteristics of the alloy surface layers [23–26]. Despite a large amount of published experimental results, optimal methods of NiTi surface treatment have yet to be developed.

The NiTi surface treatment methods to improve its corrosion resistance and biocompatibility in biological media can be arbitrarily divided into two main groups: (i) chemical and thermal treatments of NiTi implants for the selective removal of nickel from the surface layer [27–30]; (ii) synthesis of barrier layers or coatings employing different surface treatment methods, including ion-beam or ion-plasma impact of NiTi surface [19–22, 31–36].

Analysis of the literature has shown that mechanical surface treatment methods (sandblasting, mechanical polishing, etc.) do not allow the formation of corrosion resistant surface layers. The breakdown potential E_b of thus

* *Corresponding author*
Prof. Aleksandr I. Lotkov, e-mail: lotkov@ispms.tsc.ru

treated nitinol in artificial biological media is relatively low ($E_b \approx -0.1\ldots0.5$ V, (Ag/AgCl/ KCl sat.), which indicates a relatively low corrosion resistance of the material [37]. Chemical and electrochemical methods (chemical etching in acid mixtures, thermal oxidation, autoclaving in boiling water, electropolishing) result in the formation of protective surface layers, due to which E_b increases to 0.8…1.3 V [38, 39]. However, these passivation layers often have reduced resistance under cyclic thermal and mechanical loading and do not prevent material corrosion and Ni ion release.

Selection of chemical elements for surface alloying plays an important role in ensuring high biocompatibility of implants. For example, non-metal (B, C, N, O) ion implantation allows the formation of thin (30…70 nm) surface layers with increased microhardness and high corrosion resistance ($E_{tp} \approx 1.0\ldots1.2$ V) [34, 35, 40]. Ion beam treatment of NiTi surface with Si, Ti, Zr, Hf and Mo (fluence up to $2 \cdot 10^{17}$ ions/cm^2) increases corrosion resistance and improves the alloy biocompatibility [22, 34, 39]. Our recent researches [22, 41] have demonstrated the great promise of Si for this purpose. Indeed, according to the relevant literature, Si-doping of Ti alloys considerably improves corrosion resistance of these alloys in seawater [42]. At the same time the corrosion behavior of ion-implanted NiTi has not been widely studied. The aim of the present paper is to understand how NiTi surface modification with silicon affects its corrosion characteristics.

2. Materials and investigation procedure

Specimens for investigation were made of commercially pure NiTi in the form of plates 1.35×10×50 mm. The specimens were divided into three groups according to the surface treatment method: (i) mechanical polishing (NiTi-MP) with sandpaper with grit size varying from coarse to fine, (ii) chemical etching in a mixture of acids HNO_3 (65 wt %) : HF (50 wt %) = 3 : 1 parts by volume (v/v), mechanical polishing by means of a Saphire 550 grinding and polishing machine (ATM GMBH) with a gradually decreasing abrasive grit number down to 1.2...0.3 μm, and then electrolytic polishing (NiTi-EP) in a mixture of CH_3COOH (97 %) : $HClO_4$ (70 %) = 3 : 1 v/v at U = 30 V, and (iii) treatment by scheme (ii) with subsequent silicon ion implantation (NiTi-Si) using a setup DIANA-3 in the vacuum of ~10^{-4} Pa at accelerating voltage of 60 kV, pulse frequency 50 Hz and fluence $2 \cdot 10^{17}$ ions/cm^2. The specimen temperature during ion implantation did not exceed 100…150 °C. The composition, structure and morphology of the specimen surface layers were examined by optical microscopy (Axiovert 200 MAT), profilometry (New View 5000), scanning electron microscopy (LEO EVO 50 with EDS-analyzer) and Auger spectrometry (Shkhuna-2). The control experiment was performed with the use of Ti (VT1-0) and Ni (NO) plates.

The corrosion parameters (corrosion potential E_{corr}, breakdown (pitting) potential E_b and repassivation potential E_{re}, corrosion current density i_{corr}) in deaerated artificial biological media (0.9% NaCl physiological solution, artificial blood plasma of composition: 6.8 g/l NaCl, 0.4 g/l KCl, 0.2 g/l $CaCl_2$, 0.1 g/l $MgSO_4$, 2.2 g/l $NaHCO_3$, 0.126 g/l Na_2HPO_4, 0.026 g/l NaH_2PO_4 [43]) were determined with the use of procedures provided in [43]. The measurements were carried out using a thermostating three-electrode cell; the studied NiTi specimens served as the work electrodes, the area of the surface submerged into the solution was 1…2 cm^2, and the volume of the solution was 80 ml. A graphite electrode with a surface area of 20 cm^2 served as the auxiliary electrode; saturated silver-chloride electrode (Ag/AgCl/KCl sat.) was used as the reference electrode, versus which all the potentials in the work are given. Before corrosion testing, the specimen surfaces were cleaned with acetone, ethanol and rinsed with distilled water. Solutions were prepared using reagents of analytical grade and distilled water. The temperature of the solutions in corrosion testing was maintained at (37 ± 1) °C using a thermostat VT-8-1.

The E_{corr}, E_b, E_{re} and i_{corr} values for NiTi specimens in solutions were determined with the use of impulse potentiostat/galvanostat PI-50-1.1 on the basis of data obtained using potentiostatic and potentiodynamic (scan rate w = 5…10 mV/s) polarization. The average E_{corr}, E_b and E_{re} values were calculated for three identically prepared NiTi specimens from each group. The thermodynamic calculation of equilibrium activities of interaction products in the metal–solution systems were carried out using MINTEQ program [44].

3. Results and discussion

The surface morphology of NiTi-EP specimens, as examined by profilometry, is characterized by a quasiperiodic distribution of convex and concave regions with an average spacing of 5…10 μm. After modification with silicon ions, the specimen surface becomes smoother. The surface roughness parameter decreases, on the average, from 0.5…0.6 to 0.3…0.4 μm for NiTi-EP and NiTi-Si specimens, respectively. The surface topography of initial NiTi-MP specimens is governed by mechanical loading intensity during polishing. In this case, the roughness parameter is by an order of magnitude greater than, e.g., for NiTi-EP specimens, and may vary in a wide range.

The elemental composition of the surface layer of initial NiTi-MP specimens is characterized by the ratio of major alloy components Ti : Ni close to the equiatomic. The oxygen content in the natural oxide layer is determined by the time of mechanical treatment of the specimen surface and subsequent storage of the specimens in air. For NiTi-MP specimens with a newly polished surface, the oxygen content decreases from 50 to 10 at % in a relatively narrow

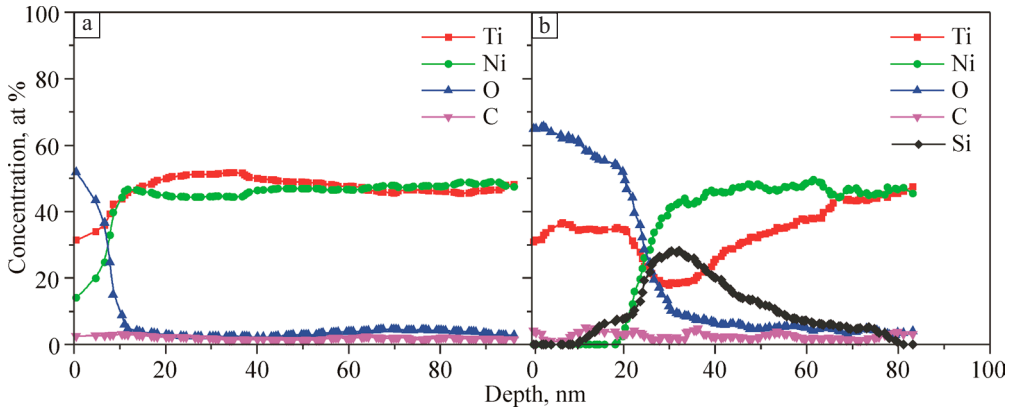

Fig. 1. Element concentration profiles for the surface layer of NiTi specimens by the Auger spectrometry data: NiTi-EP (a), NiTi-Si (b).

range of the oxidized layer thickness from 8 to 10 nm; at a greater depth the oxygen concentration reduction is less intensive. After chemical etching and electropolishing, the elemental composition of the NiTi-EP surface layer changes compared to NiTi-MP; the concentration of Ni increases from the surface to a depth of 80…100 nm (Fig. 1) due to selective removal of nickel from the surface layer in acid solutions. The main component of the ~20 nm thick surface oxide film is evidently Ti oxide which is close in composition to TiO_2.

The silicon ion beam surface modification of NiTi-EP specimens results in the formation of a silicon-containing layer in the near-surface layer 10…80 nm deep; the maximum Si concentration in the layer amounts to 30 at % at a depth of ~30…35 nm (Fig. 1). Ion implantation leads to element redistribution in the surface layer of NiTi specimens, due to which the nickel content decreases considerably in the outer layer up to 20 nm thick (Fig. 1). So, the ion beam surface modification of nitinol results in the formation of a pronounced two-layer structure, in which the surface and near-surface layers differ significantly in the concentration ratio of O, Ni and Si.

Corrosion test results show that the differences in the structure and composition of thin surface layers (of the order of tens of nanometers) of the studied NiTi specimens, which depend on the surface treatment method, exert a crucial influence on the corrosion process development. Initial NiTi-MP specimens are characterized by the narrowest (of all the studied specimens) passivation potential interval and by anodic dissolution at low potentials (Fig. 2). In the potential interval E = –0.4…0.0 V, manifested in voltammetry curves as an increase of anode current i_a up to ~$1.3 \cdot 10^{-6}$ A/cm^2, a large amount of Ni in the surface layer composition leads to its selective release into solution (Fig. 2). With further E growth, i_a increases abruptly due to corrosion rate increase accompanied by pitting failure (Fig. 3) and for the time of exposure of NiTi-MP at E_b the nickel concentration in the alloy surface layer decreases considerably (~5 times) (Table 1). Repeated cyclic polarization in the interval E = –0.7…0.5 V without surface renewal leads to almost no increase of the E interval.

Changes in the element ratio at the NiTi-EP surface layer after chemical and electrochemical treatment (Fig. 1) changes considerably the anodic process parameters as compared to NiTi-MP: the potential E_b is shifted to the domain of positive values by 0.7 V, and the decrease of i_a in the whole range of passivation potentials indicates the formation of a protective surface layer (Fig. 2). The comparison of E_b values for NiTi-EP and NiTi-Si (Table 1) with the Auger spectrometry data (Fig. 1) confirms the stability of the two-layer surface structure with the topmost layer mainly consisting of Ti oxides and Ni concentration gradually increasing to the nominal value in a relatively deep subsurface layer. The potentiostatic exposure of NiTi-EP

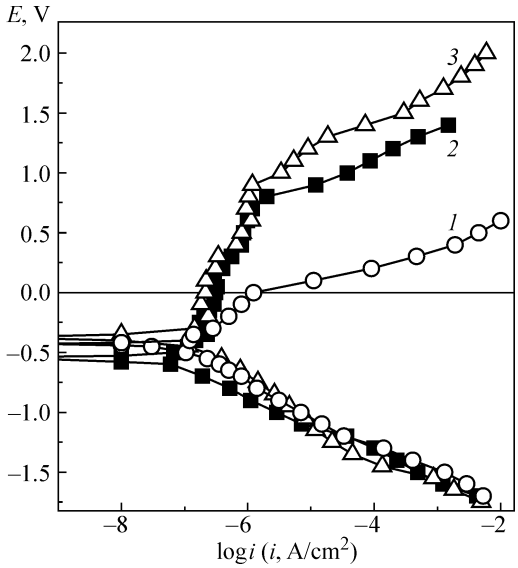

Fig. 2. Potentiostatic polarization curves of NiTi specimens in artificial blood plasma (T = 37 °C, N_2 atmosphere): NiTi-MP (*1*), NiTi-EP (*2*), NiTi-Si (*3*).

Table 1. Corrosion parameters and elemental composition of the surface layer of NiTi specimens in the initial state and after corrosion under potentiostatic conditions in artificial blood plasma (T = 37 °C, N_2 atmosphere).

Specimen	Potential, V		Elemental composition, at %							
			Initial state				After exposure at E_b for 30 min			
	E_{corr}	E_b	Ti	Ni	O	Si	Ti	Ni	O	Si
NiTi-MP	–0.43	0.0	38	39	23	–	23	8	69	–
NiTi-EP	–0.55	0.7	36	37	27	–	28	31	41	–
NiTi-Si	–0.35	0.9	39	41	19	1	39	41	18	2

at E_b does not lead to the compete failure of the protective passivation film, as a result of which nickel concentration in the near-surface layer changes insignificantly (Table 1) due to the barrier action of the outer layer.

The shift of E_b to the positive values for NiTi-Si specimens (Fig. 2) is a sign of the growing resistance of the passivation layer to failure under anodic polarization. According to profilometry and Auger spectrometry data, the reduced level of surface topography fluctuations for the modified specimens and a differentiated distribution of elements in the outer and subsurface layers (Ti-O and Ni-Ti-Si-O) cause an increase in the corrosion resistance of the alloy. In contrast to NiTi-MP and NiTi-EP, the NiTi-Si surface is much less prone to failure under potentiostatic conditions at E_b (Fig. 3).

The E_{corr} variation pattern (Table 1), which does not agree with the growing oxidation level of the NiTi-EP surface compared to initial NiTi-MP specimens, can be explained on the basis of scanning electron microscopy data about morphological changes of the surface layer during corrosion. Spotting and microcracking of the NiTi-EP surface due to corrosion failure of the protective surface layer (Fig. 3) is a result of heterogeneous topography and composition of the surface, which may lead under certain conditions to a local activation of the corrosion process and slow failure of the material beneath the passivation layer. As follows from electrochemical and electron microscopy data, the NiTi-EP surface treatment conditions allow the formation of a relatively thick passivation layer with heterogeneous morphology and composition; the mechanical characteristics of the layer differ from those in the bulk of the alloy, due to which the probability of cracking increases. The E_{corr} potentials of the modified NiTi-Si specimens are shifted to the positive values in comparison to other specimens (Table 1), which corresponds to the formation of a continuous passivation layer with enhanced cracking resistance (Fig. 3).

To investigate in detail how the modification of the alloy surface layer influences its electrochemical behavior, we compare cyclic voltammetry data for NiTi with data for titanium (VT1-0) and nickel (NO). For the NiTi-MP specimens in physiological solution and artificial blood plasma, cyclic voltammetry is characterized by a narrow range of passivation potentials –(0.6...0.1) V and by hysteresis in the interval E_{tp}–E_{re} (Fig. 4) due to very intensive pitting under cyclic variation of polarization potentials. According to the cyclic voltammetry curves of the surface-modified NiTi-Si specimens, the interval of passivation poten-

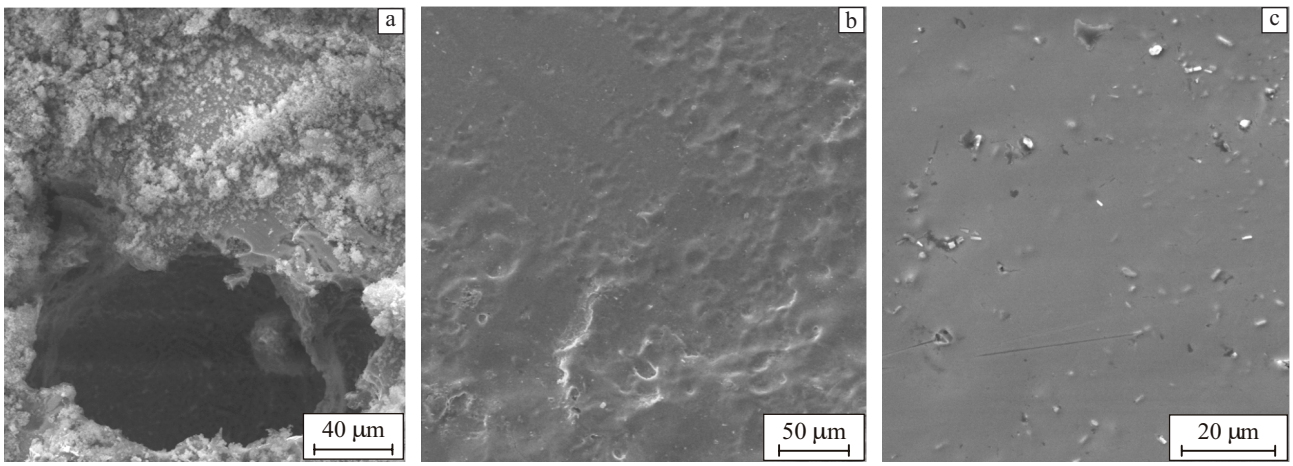

Fig. 3. SEM micrographs of the NiTi specimen surface after corrosion in artificial blood plasma (potentiostatic exposure at E_b, τ = 30 min, T = 37 °C, N_2 atmosphere): NiTi-MP (a), NiTi-EP (b), NiTi-Si (c).

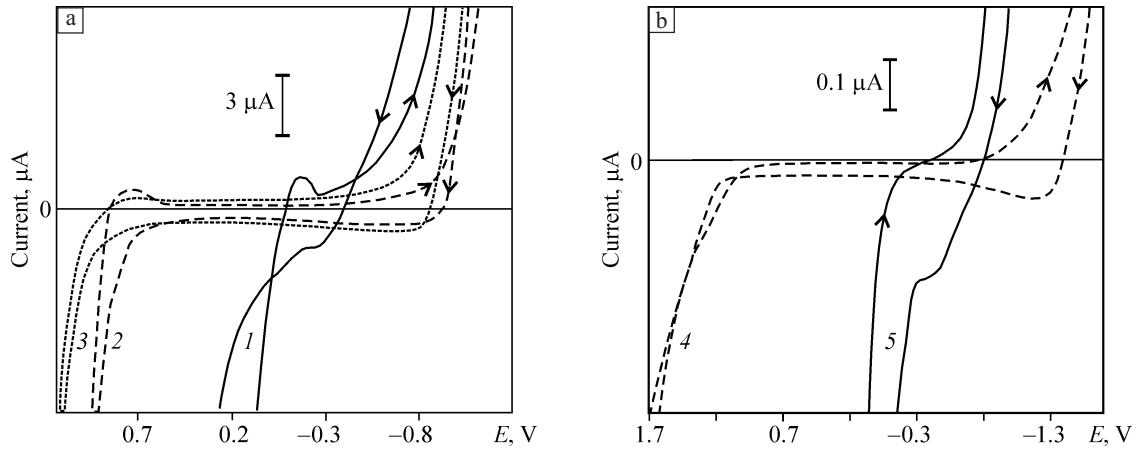

Fig. 4. Cyclic voltammetry curves of NiTi (a), titanium and nickel (b) electrodes in artificial blood plasma (T = 37 °C, N_2 atmosphere, w = 10 mV/s): NiTi-MP (*1*), NiTi-EP (*2*), NiTi-Si (*3*), Ti (VT1-0) (*4*), Ni (NO) (*5*).

tials E (–0.8…0.9 V) increases, which correlates with the data about reduced Ni content (Table 1) and growing degree of NiTi surface layer oxidation in the course of subsequent chemical, electrochemical and ion beam treatment. Unlike the NiTi-MP specimens, the cyclic voltammetry curves of the modified specimens show no hysteresis in the anodic potential region (Fig. 4) due to the large thickness of the surface passivation layer stable to breakdown at high anodic potentials and to pitting. In this case, the anodic process may be referred to water oxidation with oxygen release.

The reduced resistance of NiTi-EP specimens to microcracking of the surface layer due to its local structural heterogeneity can be determined from cyclic voltammetry data in the E_b region with anode-cathode potential sweep (Fig. 4): at $E \approx 0.7$ V there is maximum current in the cathode region which is related to the reduction of Ni^{+3} derivatives formed at high positive potentials. This effect results from the violation of continuity of the passivation layer, due to which the near-surface alloy layer with higher nickel concentration comes in direct contact with the solution. With a widening range of anodic polarization potentials under cyclic voltammetry conditions the cathode current value at $E \approx$ 0.7 V increases, which indicates that the protective action of the passivation layer decreases significantly due to corrosion cracking in cyclic variation of the potential. The near-surface layer with higher Ni content is to a lesser extent subject to passivation. The cyclic voltammetry curves of NiTi-Si specimens as well as of titanium electrodes show no above-mentioned maximum (Fig. 4) owing to the higher resistance of specimens with the modified surface to corrosion cracking, which agrees with scanning electron microscopy (SEM) data (Fig. 3).

The comparison of the electrochemical behavior of NiTi, Ni and Ti in the studied chloride-containing media suggests that the E_b value is inversely proportional to the Ni content in the surface layers of the alloy. In fact, the corrosion characteristics of NiTi-MP and nickel electrodes show close values (Fig. 4). Nickel surface passivation under cyclic voltammetry conditions causes a slight decrease in the current of hydrogen release in the region $E < -0.6$ V owing to oxide layer formation; in so doing, the transpassivation potential in chloride-containing media remains almost unchanged due to the activating influence of Cl^--ions on the anodic oxidation of metal. Unlike nickel, titanium under cyclic voltammetry conditions goes rapidly to the passive state during the formation of electrochemically inactive surface oxide which contributes to a significant E_b growth above the E_b value for NiTi-Si specimens (Fig. 4).

To explain the electrochemical results, we calculate the dependences of equilibrium activities for system Ti-Ni-Si-Cl^--H_2O on potential at physiological pH = 7.3 (Fig. 5). It follows from the analysis of the obtained dependences lg a =

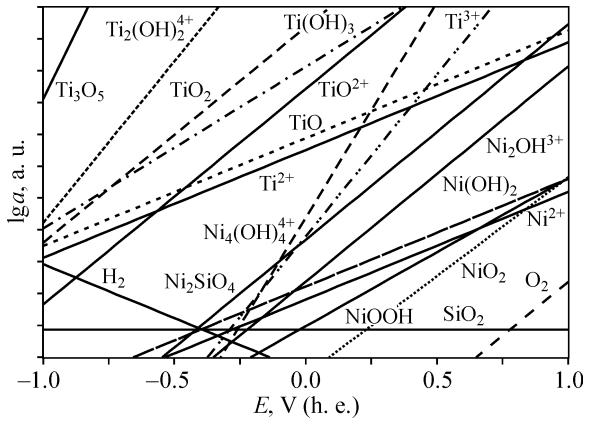

Fig. 5. Calculated logarithmic curves of equilibrium activities of oxidized forms on potential (SHE) for system Ti-Ni-Si-Cl^--H_2O ($\lg a_{Ti} = \lg a_{Ni} = \lg a_{Si} = 0$, $c^0_{Cl^-} = 0.15$ M, $I = 0.15$ M, $T = 25$ °C, pH = 7.3).

$f(E)$ that in the range of potentials close to $E_{corr} \approx -(0.1\ldots0.3)$ V (SHE), in the interaction of NiTi with chloride-containing solution, titanium mainly forms insoluble oxides and hydroxides, while nickel forms soluble ionic forms (Ni^{2+}, hydroxo-complexes). Much higher equilibrium activities of oxidized forms of titanium are due to higher reactivity of titanium with respect to oxidation reactions. This conclusion is in agreement with the experimentally measured composition of passivation layers on the NiTi surface which mainly consist of Ti oxides.

At more positive potentials $E > E_{corr}$ the fraction of soluble forms of nickel increases significantly compared to titanium (Fig. 5), which allows the breakdown effect observed in the protective oxide layer of NiTi-MP to be compared with the selective dissolution of nickel. At high positive potentials $E > E_b$ nickel has higher oxidation degrees (Fig. 5) registered in cyclic voltammetry experiments by the cathodic reduction current at $E \approx 0.7$ V (Fig. 4).

As can be seen from the curves in Fig. 5, silicon in the surface layer composition in the E_{corr} region is not involved in oxidation-reduction processes and does not form soluble species at the given pH. At $E > E_{corr}$ a poorly soluble compound Ni_2SiO_4 can be formed, which can be the cause of passive state stabilization in NiTi-Si in the region of positive potentials and thus lead to increased corrosion resistance.

4. Conclusions

The modification of nitinol surface with silicon results in the formation of a silicon-containing layer at a depth of 10…80 nm beneath the surface with the maximum silicon concentration up to 30 at % at a depth of 30…35 nm. Ion beam treatment leads to the formation of a morphologically and structurally homogeneous NiTi surface layer with the outer O-Ti (composition similar to TiO_2) and near-surface Ni-Si-Ti-O sublayers with different elemental composition.

The breakdown (pitting) potential E_b of NiTi-Si in physiological solution and in artificial blood plasma is on average equal to 0.9 V (Ag/AgCl/KCl sat.), which exceeds E_b of the NiTi specimens subjected to mechanical, chemical or electrochemical treatment. An increase in the corrosion resistance of NiTi-Si is due to reduced nickel content in the surface layer and to its more homogeneous structure.

The corrosion protective action of the silicon-modified NiTi surface layer is significantly improved which is revealed in the inhibition of pitting, spotting and microcracking.

The work was supported by the SB RAS Project No. III.23.2.1 and by the RF Ministry of Education and Science (Agreement No. 14.604.21.0031).

References

1. Anson T. Shape memory alloys—medical applications, Mater World. 1999; 7(12): 745–747.
2. Duerig T, Pelton A, Stöckel D. An overview of nitinol medical applications. Mater Sci Eng A. 1999; 273–275: 149–160.
3. Yahia H, editor. Shape memory implants. Berlin: Springer Verlag; 2000.
4. Yoneyama T, Miyazaki S, editors. Shape memory alloys for biomedical applications. Oxford: Elsevier; 2008.
5. Miyazaki S, Otsuka K. Development of shape memory alloys. ISIJ Int. 1989; 29(5): 353–377.
6. Otsuka K, Wayman CM, editors. Shape memory materials. Cambridge: Cambridge University Press; 1998.
7. Otsuka K, Ren X. Physical metallurgy of Ti–Ni-based shape memory alloys. Prog Mater Sci. 2005; 50: 511–678.
8. Samitz MH, Katz SA. Nickel dermatitis hazards from prosthesis. Brit J Derm. 1975; 92: 287–290.
9. Costa M, Jones MK. Metal carcinogenesis in tissue systems. In: Hausinger R, editor. Biochemistry of nickel. New York: Plenum Press; 1993: 47–53.
10. Saxholm HJ. Effect of nickel compounds in cell culture. In: Hausinger R, editor. Biochemistry of nickel. New York: Plenum Press; 1993: 165–173.
11. Reith A, Brogger A. Carcinogenicity and mutagenicity of nickel and nickel compounds. In: Hausinger R, editor. Biochemistry of nickel. New York: Plenum Press; 1993: 175–191.
12. Hansen RK, Stern RM. Toxicity and transformation potency of nickel compound in BHK cells *in vitro*. In: Hausinger R, editor. Biochemistry of nickel. New York: Plenum Press; 1993: 193–199.
13. Leonard A, Jacquet P. Embryotoxity and genotoxicity of nickel. In: Hausinger R, editor. Biochemistry of nickel. New York: Plenum Press; 1993: 277–286.
14. Al-Waheidi E. Allergic reaction to nickel (nitinol) orthodontic wires: A case report. Quintes Int. 1995; 26(6): 385–388.
15. Ratner BD. A perspective on titanium biocompatibility. In: Brunette DM, Tengvall P, Textor M, Thomson P, editors. Titanium in medicine: Material science, surface science, engineering, biological responses and medical applications. Berlin: Springer; 2001: 2–12.
16. Köster R, Vieluf D, Kiehn M, Sommerauer M, Kähler J, Baldus S, Meinertz T, Hamm CW. Nickel and molybdenum contact allergies in patients with coronary in-stent restenosis. Lancet. 2000; 356: 1895–1897.
17. Ries MW, Kampmann C, Rupprecht H-J, Hintereder G, Hafner G, Meyer J. Nickel release after implantation of the Amplatzer occluder. Am Heart J. 2003; 145: 737–741.
18. Wataha JC, O'Dell NL, Singh BB, Ghazi M, Whitford GM, Lockwood PE. Relating nickel-induced tissue inflammation to nickel release *in vivo*. J Biomed Mater Res. 2001; 58(5): 537–544.
19. Tan L, Crone W. Surface characterization of NiTi modified by plasma source ion implantation. Acta Mater. 2002; 50(18): 4449–4460.
20. Tan L, Dodd R, Crone W. Corrosion and wear-corrosion behavior of NiTi modified by plasma source ion implantation. Biomaterials. 2003; 24(22): 3931–3939.
21. Rautray TR, Narayanan R, Kwon TY, Kim KH. Surface modification of titanium and titanium alloys by ion implantation. J Biomed Mater Res B Appl Biomater. 2010; 93(2): 581–591.

22. Meisner LL, Lotkov AI, Matveeva VA, Artemieva LV, Meisner SN, Matveev AL. Effect of silicon, titanium, and zirconium ion implantation on NiTi biocompatibility. Adv Mater Sci Eng. 2012: 706094.
23. Meisner LL, Sivokha VP, Lotkov AI, Derevyagina LS. Surface morphology and plastic deformation of the ion implanted TiNi alloy. Physica B. 2001; 307(1–4): 251–257.
24. Tan L, Crone W, Sridharan K. Fretting wear study of surface modified Ni-Ti shape memory alloy. J Mater Sci Mater Medicine. 2002; 13(5): 501–508.
25. Levintant-Zayonts N, Kucharski S. Surface characterization and wear behavior of ion implanted NiTi shape memory alloy. Vacuum. 2009; 5(1), Suppl 1: S220–S223.
26. Zhao T, Li Y, Liu Y, Zhao X. Nano-hardness, wear resistance and pseudoelasticity of hafnium implanted NiTi shape memory alloy. J Mech Behav Biomed Mater. 2012; 9: 174–184.
27. Trépanier C, Leung T, Tabrizian M, Yahia LH, Bienvenu JG, Tanguay JF, Piron DL, Bilodeau L. Preliminary investigation of the effects of surface treatments on biological response to shape memory NiTi stents. J Biomed Mater Res B Appl Biomater. 1999; 48(2): 165–171.
28. Ryhänen J. Biocompatibility of nitinol. Minim Invasive Ther Allied Techn. 2000; 9: 99–107.
29. Michiardi A, Aparicio C, Planell J, Gil F. New oxidation treatment of NiTi shape memory alloys to obtain Ni-free surfaces and to improve biocompatibility. J Biomed Mater Res B Appl Biomater. 2006; 77(2): 249–256.
30. Shabalovskaya S, He T, Anderegg J, Schryvers DU, Carroll W, Humbeeck JV. The influence of surface oxides on the distribution and release of nickel from nitinol wires. Biomaterials. 2009; 30(4): 468–477.
31. Starosvetsky D, Gotman I. Corrosion behavior of titanium nitride coated Ni-Ti shape memory surgical alloy. Biomaterials. 2001; 22(13): 1853–1859.
32. Starosvetsky D, Gotman I. TiN coating improves the corrosion behavior of superelastic NiTi surgical alloy. Surf Coat Techn. 2001; 148(2–3): 268–276.
33. Gotman I, Ben-David D, Unger RE, Bose T, Gutmanas EY, Kirkpatrick CJ. Mesenchymal stem cell proliferation and differentiation on load-bearing trabecular nitinol scaffolds. Acta Biomater. 2013; 9: 8440–8448.
34. Sun T, Wang L-P, Wang M. (Ti, O)/Ti and (Ti, O, N)/Ti composite coatings fabricated via PIIID for the medical application of NiTi shape memory alloy. J Biomed Mater Res B Appl Biomater. 2011; 96(2): 249–260.
35. Barcos R, Conde A, de Damborenea J, Puertolas J. Effect of nitrogen ion implantation on *in vitro* corrosion behaviour of NiTi. Revista Metal. 2008; 44(4): 326–334.
36. Zhao T, Li Y, Zhao X, Chen H, Zhang T. Ni ion release, osteoblast–material interactions, and hemocompatibility of hafnium-implanted NiTi alloy. J Biomed Mater Res B Appl Biomater. 2012; 100(3): 646–659.
37. Shabalovskaya S, Rondelli G, Anderegg J, Xiong JP, Wu M. Comparative corrosion performance of black oxide, sandblasted, and fine-drawn nitinol wires in potentiodynamic and potentiostatic tests: effects of chemical etching and electropolishing. J Biomed Mater Res B Appl Biomater. 2004; 69(2): 223–231.
38. Shabalovskaya S, Rondelli G, Undisz A, Anderegg JW, Burleigh TD, Rettenmayr ME. The electrochemical characteristics of native nitinol surfaces. Biomaterials. 2009; 30(22): 3662–3671.
39. Milosev I, Kapun B. The corrosion resistance of nitinol alloy in simulated physiological solutions: Part 1: The effect of surface preparation. Mater Sci Eng. 2012; 32(5): 1087–1096.
41. Psakhie SG, Meisner SN, Lotkov AI, Meisner LL, Tverdokhlebova AV. Effect of surface alloying by silicon on the corrosion resistance and biocompatibility of the binary NiTi. ASM Int J Mater Eng Perform. 2014; 23(7): 2620–2629.
42. Jiang Z, Dai X, Middleton H. Effect of silicon on corrosion resistance of Ti-Si alloys. Mater Sci Eng B. 2011; 176(1): 79–86.
43. ISO 10993-15:2000 Biological evaluation of medical devices: Part 15: Identification and quantification of degradation products from metals and alloys; 2000.
44. Felmy A, Girvin D, Jenne E. MINTEQ: A computer program for calculating aqueous geochemical equilibria. Washington: US Environmental Protection Agency; 1984.